Electron-strain interaction in the singlet-ground-state compound TmSb

Shigeki Nimori

Tsukuba Magnet Laboratory, National Institute for Materials Science, 3-13 Sakura, Tsukuba 305-0003, Japan

Mitsuo Kataoka

Department of Material Research, Graduate School of Iwaki Meisei University, 5-5-1 Iino Chuodai, Iwaki, Fukushima 970-8551, Japan

Terutaka Goto

Graduate School of Science and Technology, Niigata University, Niigata 950-2181, Japan

Giyuu Kido

Nanomaterials Laboratory, National Institute for Materials Science, 3-13 Sakura, Tsukuba 305-0003, Japan

We studied the electron-strain interaction for the singlet-ground-state compound TmSb using ultrasonic measurements to observe the quantum oscillation of elastic constants. Their oscillatory intensity was highly anisotropic depending on the applied field direction, and on the propagation and polarization direction of the ultrasonic wave. This anisotropy has been explained by response theory based on effective-mass approximation. Our analysis provides coupling coefficients between itinerant electrons and the lattice system. From the width of the Fermi-surface splitting, we obtained exchange interactions between localized and itinerant electrons.

I. INTRODUCTION

Rare-earth monopnictides have been used as typical compounds to verify physical models because they crystallize simple NaCl crystal structures. These monopnictides, for example, enabled us to develop a crystalline electric-field (CEF) theory.[1] This simple structure is also useful in the experimental investigation of their physical properties because this structure facilitates analysis and discussion. Rare-earth monopnictides show dramatic behavior originating in the interaction between localized f electrons and conduction electrons.[2,3] The major reason for such behavior is that their physical properties are influenced by this interaction due to a low carrier concentration for semimetallic or semiconductive characteristics.[4,5] Because of the characteristics of low carrier concentration, the sample dependence becomes significant. Thus, it is indeed important for the investigation of these compounds to use high-quality single crystals. Recently, high-quality single crystals of rare-earth monopnictides have been obtained by the Bridgman method using a high-frequency hearth.[6]

We measured the acoustic de Haas–van Alphen (a-dHvA) effect, observing the quantum oscillation of ultrasonic waves for TmSb in the C_{11} mode. We used a high-quality single crystal and determined the complete structure of the Fermi surface.[7] Investigations along different field angles indicate the structure of the Fermi surface, the cyclotron effective mass, and the Dingle temperature. Oscillatory intensity contains information on electron-strain interaction. Analysis of results in the dHvA measurements is rather complex because it involves the relationship between modulation and the applied field. The acoustic dHvA effect is obviously a more elegant way to investigate electron-phonon interactions than the standard modulation method because the a-dHvA effect

does not require a modulation field. The absence of this modulation field makes it easy to analyze electron-strain interactions. The modulation field generates Joule heating at metallic parts of the experimental equipment, which is an obstacle for low-temperature measurements. We previously reported the high anisotropic behavior of the a-dHvA oscillatory intensity in the longitudinal C_{11} mode in TmSb.[7] To explain the anisotropic behavior of the C_{11} mode, we use the *response theory* based on effective-mass approximation[8] in this paper. In the a-dHvA measurement series for other rare-earth monopnictides,[9–11] the anisotropic oscillatory intensity of the elastic constant was observed. An analysis by the response theory in rare-earth monopnictides LaAs, CeAs, and CeBi (Refs. 12–14) and the metallic compound LaB_6,[15] measurements are restricted in either the longitudinal or the transverse mode except for rare-earth hexaboride LaB_6. To proceed to the next step in understanding electron-strain interactions of rare-earth monopnictides, we conducted the a-dHvA measurement of the transverse C_{44} mode. We report and discuss longitudinal and transverse a-dHvA measurements. This paper is a complete study of electron-strain interactions using response theory and provides much worthwhile information. We obtained the electron-strain interaction for up and down spins independently due to the spin-splitting Fermi surface in TmSb.

We also review the exchange interactions between f electron and conduction electrons, which govern the main properties of rare-earth monopnictides. We focused on TmSb and PrSb. The CEF ground state of Tm and Pr ions is singlet in TmSb and PrSb and nonmagnetic in zero fields. Although magnetic momentum disappears in zero fields, a large magnetization is induced by hybridization from the CEF excited states to the ground state.[16–21] We measured the dHvA effect on the hypothesis that the field-induced moment of f elec-

trons influences conduction electrons and causes some change in the Fermi surface. A detailed study of the Fermi surface has been done up to 8 T in PrSb,[9] but no change in the Fermi surface was observed by the applied field. We measured the dHvA effect on the principal axis of the cubic structure up to 25 T using a hybrid magnet.[22,23] Results indicate a small change in the Fermi surface.[24] We inferred that hybridization by the applied field occurs in a lower applied field if energy difference between the ground and the first excited state of the CEF (ΔE) is smaller. In a zero field, ΔE is 25 K for TmSb,[25–27] but 75 K for PrSb.[28–30] The magnetic momentum of Tm^{3+} is estimated to be 7.57 μ_B by the Hund rule. This is larger than that of PrSb, which corresponds to 3.58 μ_B. If we assume that the influence on conduction electrons by magnetization is proportional to the magnetic momentum, the factor for TmSb is doubled compared to that of PrSb. As envisioned, we found exchange splitting of the Fermi surface in TmSb.[7] Interaction coefficients between f electrons and conduction electrons have been estimated elsewhere[31] and preliminary results obtained. Here, we take into account the magnetic susceptibility in estimating the interactions.

We present experimental results for the a-dHvA effect for TmSb, emphasizing that analysis by the response theory can explain anisotropic oscillatory intensity. In Sec. II, we describe single-crystal growth and characterization of crystals used for measurements. In Sec. III, we review exchange interaction and the application of response theory to experimental results. We also study the intensity of the longitudinal C_{11} and transverse C_{44} modes originating in the anisotropic electron-strain interaction. In Sec. IV, we discuss information acquired using the response theory.

II. EXPERIMENT

We grew a single crystal of TmSb that was 14 mm in diameter and 20 mm long by the Bridgman method in a closed tungsten crucible.[6] We checked the stoichiometry of the sample by inductively coupled plasma atomic emission spectroscopy. The deviance from the stoichiometry was estimated to be 1% at most. Samples for measuring the acoustic dHvA effect were prepared by cleaving samples along the (100) plane into $2 \times 2 \times 4$ mm^3 rectangles.

To detect the quantum oscillation of sound velocity in a magnetic field, we used an ultrasonic apparatus based on phase comparison.[32] A piezoelectric transducer $LiNbO_3$, which has high electric-mechanical coupling, was used for both the ultrasonic generator and detector. The frequency of sound waves was varied between 30 and 75 MHz, and the ultrasonic wave pulse width was fixed at about 1.0 ms. The resolution of sound velocity is $\Delta n/n = 10^{-7}$, sufficient to detect quantum oscillation in ultrasound. The acoustic dHvA effect in TmSb was measured using the transverse C_{44} and longitudinal C_{11} modes. The sample was cooled to 0.5 K using a circulation ^{3}He refrigerator.[33,34] Magnetic fields were generated by a superconducting magnet up to 8 T. To determine the angular dependence of the dHvA frequency and oscillation intensity, the sample orientation was adjusted by a two-circle goniometer.[35] We measured magnetization to take
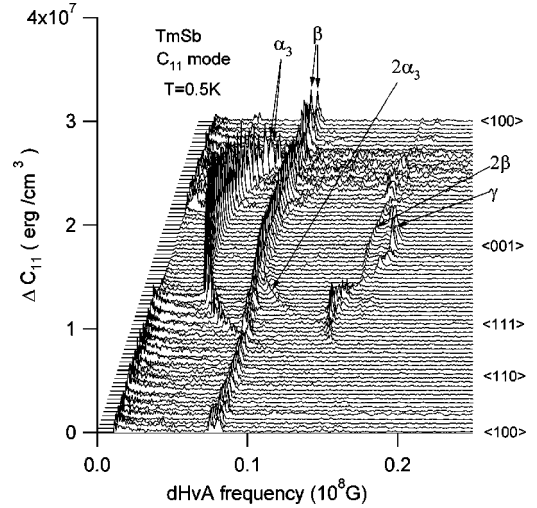
FIG. 1. Angular dependence of the FFT spectrum on TmSb in the C_{11} mode acoustic dHvA oscillation.

into account the internal field, given by $B = H + 4\pi(1 - N)M$, where $N(=0.34)$ represents the demagnetization factor of the sample and M is the total magnetic moment per unit volume.

III. RESULTS

A. Exchange interaction

Figure 1 shows the angular dependence of the fast Fourier-transformation (FFT) spectrum for the acoustic dHvA oscillation in the C_{11} mode. The relationship between the applied field and propagation direction of the ultrasonic wave in measurement is shown in Fig. 2. The dHvA frequencies of TmSb consist of three main branches indicated as α, β, and γ, named from the reference compound LaSb.[5,9,36] Electron α branches, forming ellipsoids located at the three X points, are ordinarily derived from the d orbit with t_{2g} character on Tm. β and γ hole surfaces are located at the Γ point of the zone center, which mainly consist of the p orbit with the Γ_8 character on Sb. The β surface is almost spherical but the γ surface is slightly elongated along the fourfold axes. Double peaks of α and β in Fig. 1 show the spin split of the Fermi surface.
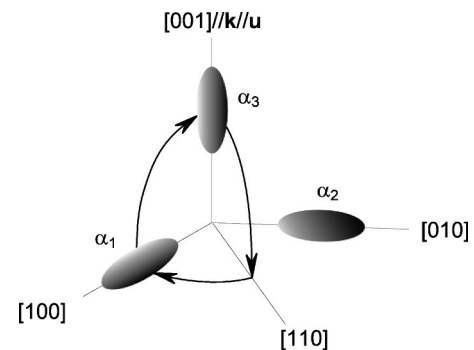
FIG. 2. Relationship of propagation vector **k** and polarization vector **u** of the ultrasonic wave in the C_{11} measurement.

TABLE I. Fermi energies E_F, cyclotron effective-mass ratios m^*, and Dingle temperatures T_D for split α and β branches of TmSb. Suffixes l and h indicate the lower-frequency and higher-frequency branches of split branches. Effective-mass ratios for α surfaces were acquired from the cyclotron motion of the shortest orbit with ellipsoidal shapes. Fermi energies of β branches are averages for β^l and β^h.

	E_F (K)	m^* ($=m_{eff}/m_0$)	T_D (K)
α^l	3.60×10^3	0.12	4.7
α^h	3.27×10^3	0.14	4.7
β^l	5.23×10^3	0.16	2.5
β^h	5.23×10^3	0.17	2.5

The dHvA frequencies remain within 0.2×10^8 G, estimated to be roughly ten times smaller than most metallic compounds. From the cross-sectional area of the Fermi surface, the carrier number is estimated by $n=7.4\%$ per Tm ion in TmSb, about quintuple compared with $n=1.4\%$ per La ion in LaSb.[5,9,36]

In the spin split of the up and down spins of the Fermi surface, the dHvA frequencies are obtained by the FFT analysis. The FFT analysis is usually conducted in a limited field region where oscillations are observed. In analysis, we assume that oscillations continue infinitely, and as a result, the frequency observed by the FFT analysis corresponds to the value extrapolated to zero magnetic fields. Fortunately, in many cases, the Zeeman split grows proportionally to the applied field, or the split width is too small to appear in the FFT spectrum. Thus, we must observe a single frequency for the up and down spins of the Fermi surfaces. In TmSb, however, the large steep increase in field-induced magnetization drastically changes the curvature for magnetization in the field region from 5 T to 10 T. Thus, the Zeeman split develops nonproportionally to the applied field, and different dHvA frequencies of the up and down spins are observed in the FFT spectrum.

From the split width, we obtain exchange interaction coefficients between conduction electrons and localized f electrons. Using a spin-split width of $2\Delta H_S$ in the FFT spectrum, we describe the exchange interaction of J_{sf} as follows:

$$\mu_B 2\Delta H_S = \pi s A J_{sf}\left\{ \langle S_f\rangle_{\mathbf{B}_0} - \left(\frac{\partial\langle S_f\rangle}{\partial\mathbf{B}}\right)_{\mathbf{B}_0}\mathbf{B}_0\right\}. \quad (1)$$

Here

$$A=\left(\frac{m_x m_y m_z/m_0^2}{m_x\beta_x^2+m_y\beta_y^2+m_z\beta_z^2}\right)^{1/2}, \quad (2)$$

where β_i and m_i ($i=x,y,z$) are direction cosines and effective masses. S_f represents the absolute spin in a unit of $\hbar$. We take into account the anisotropy of effective mass represented by A, compared to previous reports.[7,31] We summarize Fermi energies E_F, cyclotron effective-mass ratios $m^*=m_{eff}/m_0$, and Dingle temperatures T_D in Table I. Suffixes l and h denote the lower- and higher-frequency branches.

TABLE II. Exchange interactions (in eV) between localized f electrons and conduction electrons along three principal axes in TmSb.

	$\langle100\rangle$	$\langle110\rangle$	$\langle111\rangle$
α	5.5×10^{-2}	5.3×10^{-2}	5.4×10^{-2}
β	8.4×10^{-2}	7.3×10^{-2}	9.0×10^{-2}
γ		1.4×10^{-2}	4.6×10^{-2}

The resultant exchange interaction coefficients summarized in Table II, were obtained only in the three principal axes of a cubic structure. To calculate the exchange interaction, we require absolute magnetization as shown in Eq. (1) and measured magnetization along the three principal axes. The exchange interaction of the β branch is larger than α and γ branches in $\langle100\rangle$, $\langle110\rangle$, and $\langle111\rangle$ (see Table II). The result indicates that conduction electrons, which mainly consist of the p orbit on Sb, interact strongly with localized electrons because of the similar symmetry of the wave function. For the β branch, the anisotropy for the exchange interaction was observed, while α is almost independent of applied fields. The exchange interaction enhanced in $\langle111\rangle$ for the γ branch is the same behavior as the β branch. This behavior is caused by the large magnetization in $\langle111\rangle$ among the three principal axes. In the $\langle100\rangle$ direction, the oscillatory intensity of the γ branch was not sufficient, so splitting of the γ branch was unclear.

B. Electron-phonon interaction

1. Response theory

To explain the anisotropic oscillatory intensity of elastic constants, we used response theory.[8] A sound wave induces lattice deformation in the crystal, changing the cross-sectional area of the Fermi surfaces, i.e., free energy. The oscillatory part of the elastic constant is obtained by the second derivative of free energy with respect to strain component ε_{ij}. In our experiment, $H_S(\beta)/H$ is sufficiently large to neglect the strain dependence of $F_S(H,\beta,0)$ and the second term containing $H_S(\beta)/H$ in Eq. (45) of Ref. 8. Consequently, oscillatory parts of the elastic constant are

$$C_{ij:i'j'}(H,\beta,0)=-F_S(H,\beta,0)\Lambda_{ij}(\beta)\Lambda_{i'j'}(\beta)$$
$$\times\left(\frac{H_S(\beta)}{H}\right)^2\cos\left(\frac{H_S(\beta)}{H}+\frac{\pi}{4}\eta\right). \quad (3)$$

After Fourier analysis in Eq. (3), the oscillatory intensity remains as

$$|\Delta C_{ij:i'j'}(H,\beta,0)|$$
$$=\left|F_S(H,\beta,0)\Lambda_{ij}(\beta)\Lambda_{i'j'}(\beta)\left(\frac{H_S(\beta)}{H}\right)^2\right|. \quad (4)$$

Factor $F_S(H,\beta,0)$ is eliminated by dividing the above equation by Eq. (41) or Eq. (42) in Ref. 8, which corresponds to

the longitudinal or transverse sound wave, respectively. We extract the area coefficient $\Lambda_{ij}(\beta)$ from the oscillatory intensity of elastic constant C_{ij}.

Response theory indicates that area coefficient $\Lambda_{ij}(\beta)$ consists of deformation, rotation, and a multiband term:

$$\Lambda_{ij}(\beta) = \Lambda_{ij}^d(\beta) + \Lambda_{ij}^r(\beta) + \Lambda_{ij}^m. \tag{5}$$

Deformation coupling $H = g_{zz} p \varepsilon$ of the longitudinal C_{11} mode with strain ε_{zz} leads to the deformation term:

$$\Lambda_{zz}^d(\beta) = \frac{g_{zz}}{6}\left(\frac{2m_z\beta_z^2 - m_x\beta_x^2 - m_y\beta_y^2}{m_x\beta_x^2 + m_y\beta_y^2 + m_z\beta_z^2}\right). \tag{6}$$

In the transverse C_{44} mode with strain ε_{zz}, deformation coupling $H = g_{xy} p_x p_y \varepsilon_{xy}(\sqrt{m_x m_y})$ yields the deformation term

$$\Lambda_{xy}^d(\beta) = g_{xy}\frac{\sqrt{m_x m_y}\beta_x\beta_y}{m_x\beta_x^2 + m_y\beta_y^2 + m_z\beta_z^2}. \tag{7}$$

Here, g_{ij} signifies the parameter implying the interaction between the conduction electron and elastic strain, β_i the direction cosine of the applied magnetic-field direction, and m_i the effective mass of the ellipsoidal Fermi surface. The transverse C_{44} mode, which propagates along the [100] axis with the polarization vector parallel to [010], induces pure strain ε_{xy} and the lattice rotation ω_{xy}. This lattice rotation also changes the cross-sectional area of the Fermi surface with an anisotropic shape, because the applied field direction is fixed by the superconducting magnet. The rotation term is calculated as

$$\Lambda_{xy}^r(\beta) = \frac{(-m_x + m_y)\beta_x\beta_y}{m_x\beta_x^2 + m_y\beta_y^2 + m_z\beta_z^2}. \tag{8}$$

The rotation term is a pure geometric effect, free from deformation coupling. Because the longitudinal mode does not include lattice rotation, the rotation term is relevant only for the transverse mode.

Regarding the multiband effect, band energy is changed by the elastic strain of the sound wave. In a system with a multiband structure, electrons in a band are transferred to other bands under the constraint of a fixed electron number. This process causes the Fermi level to change, changing the cross-sectional area. Response theory considers this as a multiband effect. The multiband term Λ_{ij}^m does not depend on the field direction.

Here, we infer the spin reduction factor in detail. The spin factor is usually described as

$$R_s = 2\cos\left(\frac{1}{2}\pi s g m^*(\beta, \xi_{ij})\right), \tag{9}$$

where s represents the number of harmonic oscillations. The spin factor is multiplied by the oscillatory intensity. When the effective mass is small, that is, $gm^* \ll 1$, the dHvA oscillatory amplitude is not so influenced by the spin factor. In rare-earth monopnictides, however, the effective mass ratio holds at 10^{-1}–10^{-2}. So, the spin reduction factor is not
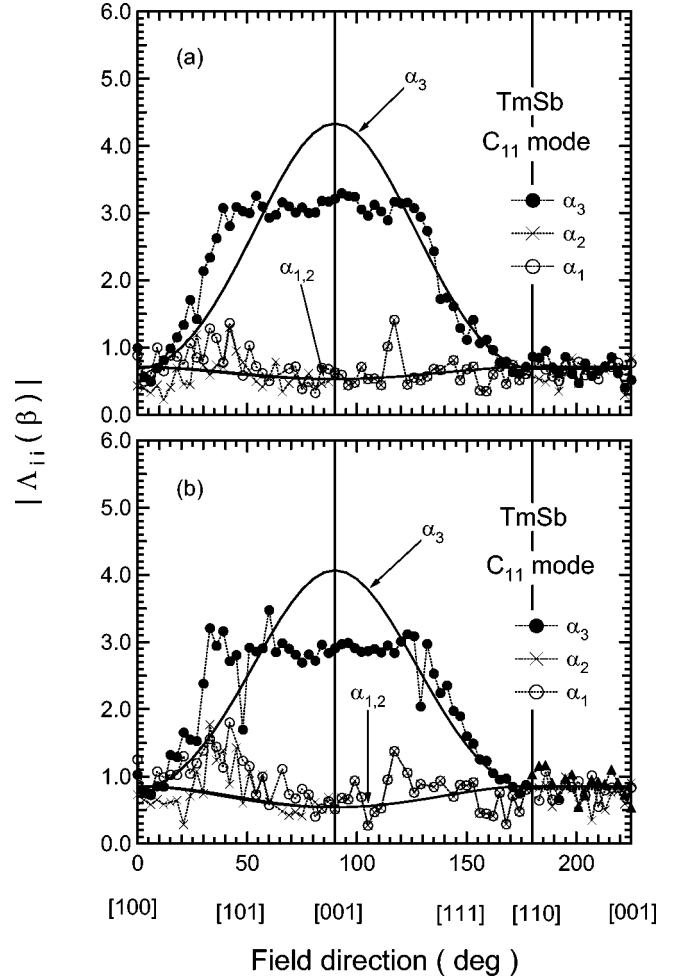
FIG. 3. Angular variation of area coefficients for spin-split α surfaces measured for the C_{11} mode. Solid lines are theoretical fits. (a) Lower-frequency branches; (b) higher-frequency branches.

negligible. In this stage, however, we assume $R_s = 1$ for simplicity. The spin factor is detailed elsewhere.

Analysis is restricted in $g = 2.00$, which is the value for free ions. Taking into account enhancements by the spin-orbit interaction or other many-body effects, we must take into account the g factor in the calculation. See Sec. IV. We conducted analysis for α and β branches because they are ellipsoidal and spherical, which is fully calculated for the geometric factor without any assumption.

2. C_{11} mode

From FFT spectra intensities, we obtained $\Delta C_{11}/C_{11}$ using the absolute elastic constant $C_{11} = 1.74 \times 10^{12}$ erg/cm^3. The longitudinal C_{11} mode related to elastic strain ε_{zz} detects area coefficient $\Lambda_{33}(\beta)$ for α_3 surfaces and $\Lambda_{11}(\beta)$ [$= \Lambda_{22}(\beta)$] for $\alpha_1(\alpha_2)$ surfaces. $\Lambda_{33}(\beta)$ means the area coefficient with the field parallel to the major axis of the ellipsoidal surface, and $\Lambda_{22}(\beta)$ or $\Lambda_{11}(\beta)$ denotes the minor axis parallel to the field.

Figure 3 shows the angular variation of area coefficients obtained by the C_{11} mode. The quantum oscillation intensity of three α branches differs significantly. Only Λ_{33} of α_3 was
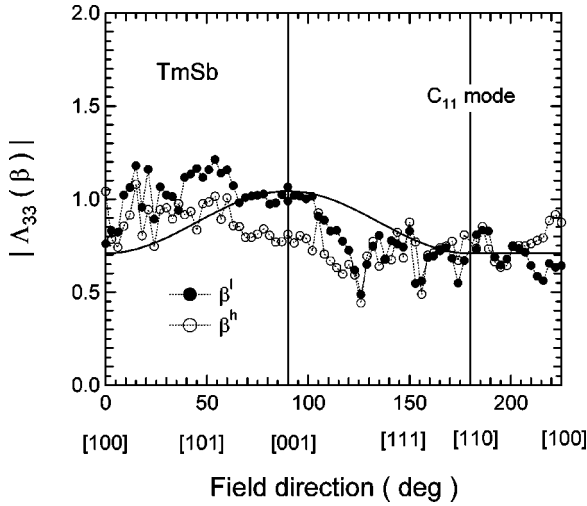
FIG. 4. Angular variation in area coefficients for β surfaces measured for the C_{11} mode. Superscripts l and h represent lower- and higher-frequency branches. The solid line is a theoretical fit by response theory.

observed to have a large intensity. Poor intensity was detected for α_1 and α_2 in the plane perpendicular to the propagation direction. Solid lines in Fig. 3 represent curves calculated by response theory, where we used a set of parameters $g_{11}=g_{22}=-0.36$ and $g_{33}=7.3$ for the deformation coupling and for multiband terms $\Lambda_{11}^m(\beta)=\Lambda_{22}^m(\beta)=0.75$ and $\Lambda_{33}^m(\beta)=1.9$ in the high-frequency α branch (α^h). In the low-frequency α branch (α^l), $g_{11}=g_{22}=-0.63$, $g_{33}=6.5$ and $\Lambda_{11}^m(\beta)=\Lambda_{22}^m(\beta)=0.75$, and $\Lambda_{33}^m(\beta)=1.9$ were obtained. The relatively large deformation coupling constant g_{33} and multiband term $\Lambda_{33}^m(\beta)$ for surfaces correspond to the large oscillation intensity of α_3 in the C_{11} mode. Calculation based on response theory well reproduced experimental results except for the angular-independent part of α_3 in the [001] direction. This inconsistency may be caused by the spin factor and may show the importance of the spin factor in TmSb.

Angular variation of the β branch is shown in Fig. 4. Since the β hole surfaces are almost spherical, we expect isotropic angular variations of curvature factor $S''=2\pi$ and the effective mass. Obtained deformation-potential couplings and multiband terms are $g_{ii}(i=1,2,3)=0.67$ and $\Lambda_{ii}^m(i=1,2,3)=0.82$. In Fig. 4, we show a fitting curve for β^h and β^l because the difference in $\Lambda_{33}(\beta)$ for β^h and β^l surfaces is not significant. The fine structure in experimental results is not explained at this stage. Intensity on the (010) plane is relatively larger than that on the $(1\bar{1}0)$ plane, i.e., the same behaviors in the α branch. We note that the enhancement in the (010) plane in the β surface is described by the analysis, taking into account the spin factor. Details of analysis are reported elsewhere.

3. C_{44} mode

The experimental setting of ultrasound measurement is shown in Fig. 5. Figures 6 and 7 show area coefficients of the transverse mode for α^l and α^h surfaces, where the abso-
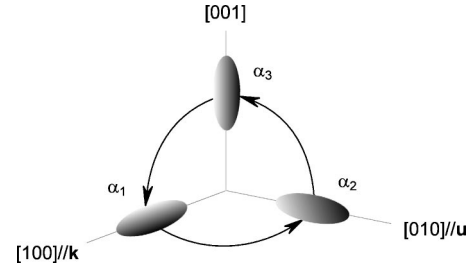
FIG. 5. Relationship of propagation vector **k** and polarization vector **u** of the ultrasonic wave in a transverse C_{44} measurement.

lute elastic constant $C_{44}=2.38\times10^{11}$ erg/cm^3 is used for calculations. The C_{44} mode propagating with [100] direction with polarization [010] induces pure strain ε_{xy} and lattice rotation ω_{xy}. Area coefficient $\Lambda_{12}(\beta)$ is detected for the α_3 surface, $\Lambda_{23}(\beta)$ for α_1, and $\Lambda_{31}(\beta)$ for α_2. When the magnetic field is applied to the (100) plane perpendicular to the propagation direction of the C_{44} mode, both the deformation term in Eq. (7) and the rotation term in Eq. (8) disappear because of direction cosine $\beta_x=0$. A similar disappearance is expected in the (010) plane perpendicular to the polarization direction of the C_{44} mode because $\beta_y=0$. The multiband term of α Fermi surfaces, located at X point, disappears due
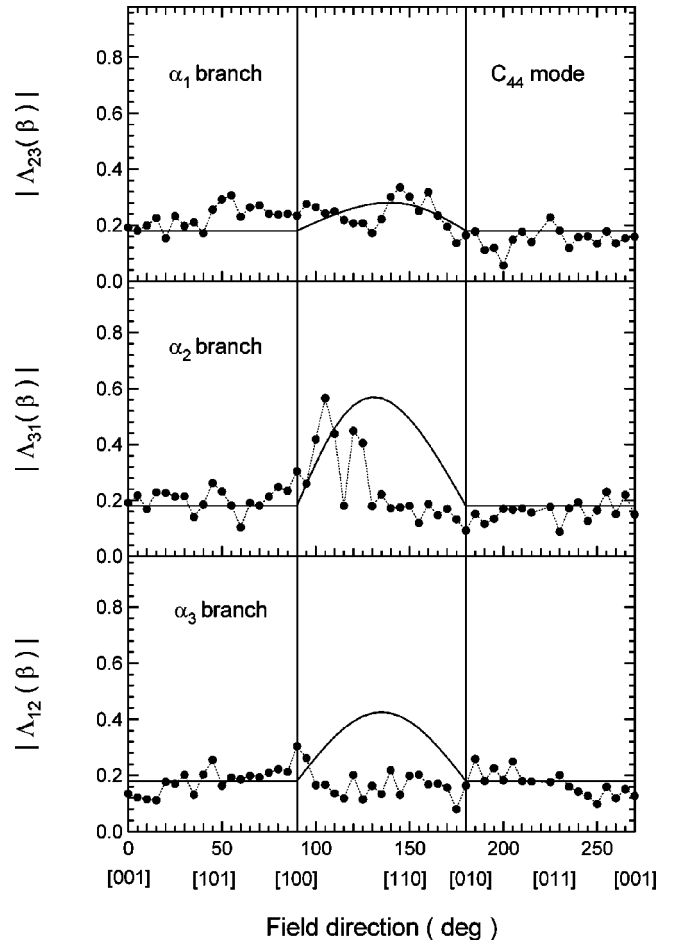
FIG. 6. Angular variation in area coefficients for low-frequency α surfaces measured for the C_{44} mode. Solid lines are calculated by response theory.
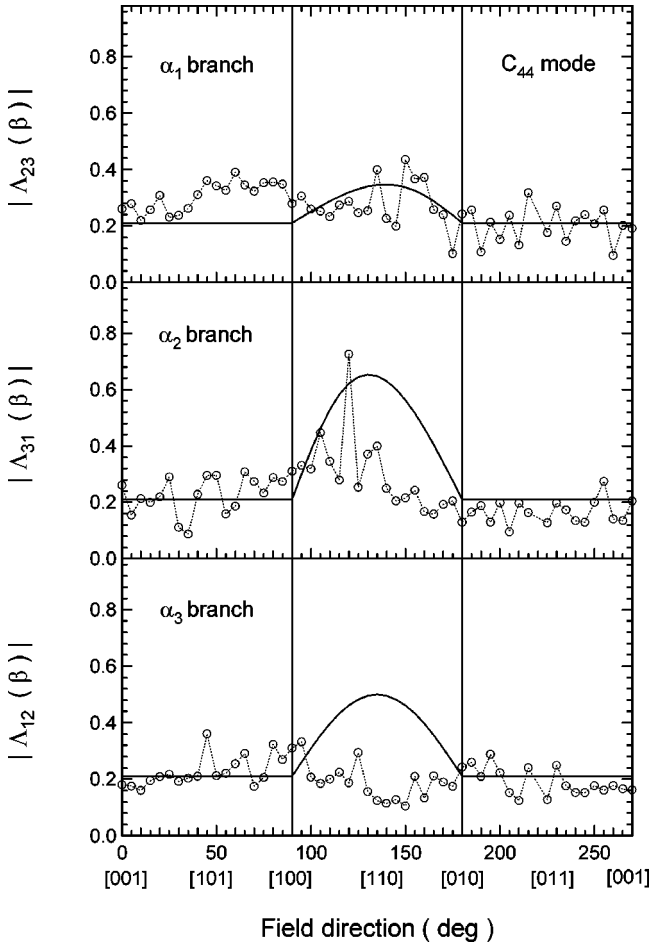
FIG. 7. Angular variation in area coefficients for high-frequency α surfaces measured for the C_{44} mode. Solid lines are calculated by response theory.

FIG. 8. Angular variation in area coefficients for β surfaces measured for the C_{44} mode. Solid lines are calculated by response theory.

to the tetragonal symmetry at the X point of the Brillouin zone. Consequently, response theory predicts that the oscillation disappears on the (100) and (010) planes. Deformation, rotation, and multiband terms are relevant on the (001) plane. As shown in Figs. 6 and 7, the oscillation of α_1 and α_2 should be detectable with large intensity only on the (001) plane. A rather small intensity is detectable on the (100) and (010) planes, corresponding to the background signal level. Experimental results are qualitatively consistent with calculation by response theory. For fitting to experimental results, we use deformation-potential coupling constants $g_{12} = g_{31} = 0.49$ for the α^l branch and $g_{12} = g_{31} = 0.58$ for the α^h branch. In general, the oscillation intensity of the C_{44} mode was weaker than that of the C_{11} mode, originating in the difference of the bulk modulus between longitudinal and transverse modes. This indicates that off-diagonal $\Lambda_{ij}(\beta)$ is small, although diagonal $\Lambda_{ii}(\beta)$ has large values as mentioned in the C_{11} mode analysis.

We observed clear evidence for the rotation term in the C_{44} mode. As mentioned above, response theory holds that the rotation, deformation, and multiband terms are concurrently detectable only on the (001) plane. Among the three terms, the multiband term is independent of the field angle, and the deformation term has a symmetry curvature from
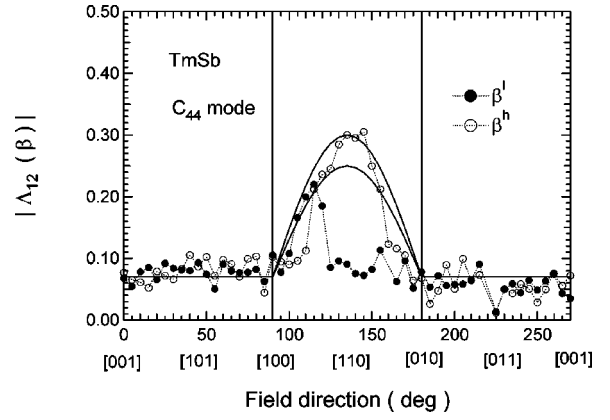
[100] to [010] on the (001) plane. Accordingly, the rotation term causes asymmetric curvature on the (001) plane. Note the asymmetric intensity for α_1 and α_2 in Figs. 6 and 7 on the (001) planes. We detected the asymmetric oscillatory intensity of Λ_{xy} of α_1 and α_2 in Figs. 6 and 7, but they were not very clear due to the small intensity for the C_{44} mode. Our study is, to our knowledge, the first case to observe the contribution of the rotation term in the transverse C_{44} mode. For α_3, rotation term $\Lambda_{12}^r(\beta)$ disappears because of the tetragonal symmetry of the α surface, suggesting a poor intensity for α_3; the oscillatory intensity α_3 was rather small compared to α_2 and α_1 in Figs. 6 and 7.

Figure 8 shows the angular variation of $\Lambda_{12}(\beta)$ for β^l and β^h surfaces. The rotation term of Eq. (8) disappears due to the spherical shape of the β surface by direction cosine $\beta_i = 0$. Thus, on the (001) plane, both deformation and multiband terms appear in the area coefficient. On the (100) and (010) planes, only the multiband term remains. Solid lines are curves calculated for β^l and β^h, where $g_{12} = g_{23} = g_{31} = 0.36$ and $\Lambda_{12}^m(\beta) = \Lambda_{23}^m(\beta) = \Lambda_{31}^m(\beta) = 0.07$ were used for the β^l surface. For the β^h surface, we obtained $g_{12} = g_{23} = g_{31} = 0.46$ and $\Lambda_{12}^m(\beta) = \Lambda_{23}^m(\beta) = \Lambda_{31}^m(\beta) = 0.07$, but experiments and theory do not agree satisfactorily. Disagreement on the (001) plane appears to originate from the spin factor. We infer that the multiband term could be extinguished due to the high symmetry of the β surface, which lies at Γ point in the Brillouin zone. We thus consider that $\Lambda_{ij}^m(\beta) = 0.07$ is not significant, and almost corresponds to the background level.

IV. DISCUSSION

We discuss deformation-potential coupling parameters g_{ij} and their significance. The relationship between the Fermi energy and deformation-potential coupling is quantitatively clarified below. Deformation coupling g_{ij} in TmSb, where the Fermi energy (E_F) of α and β surface is estimated at 3×10^3 K and 5×10^3 K, is held in the region between 0.3 and 10. In LaAs, g_{ij} is in the region between 8 and 16, where the Fermi energy is estimated to be 1×10^3 K. Absolute g_{ij}

correlates with E_F, i.e., deformation-potential interaction decreases with increasing E_F. In normal metal LaB_6, g_{ij} is smaller than 1 for the Fermi surface of $E_F = 1.5 \times 10^4$ K.[15] These results show that deformation coupling g_{ij} indicates the sensitivity of free energy of conduction electrons to deformation by sound waves near the Fermi surface.

The oscillatory intensity of the a-dHvA effect is enhanced when an ultrasound wave propagates along the long axis of ellipsoidal α in the C_{11} mode. That is, quantum oscillation is easily detected when propagation vector (**k**) is perpendicular to the smallest cross-sectional area of the Fermi surface, since the susceptibility of free energy to modulation by the sound wave is enhanced by the large bulk modulus of the longitudinal mode. The 10 times larger area coefficient in C_{11} compared to C_{44} could be explained by the same mechanism. Since the C_{11} mode induces volume strain, $\varepsilon_B = \varepsilon_{xx} + \varepsilon_{yy} + \varepsilon_{zz}$, the bulk modulus is much larger than the transverse mode.

Before response theory, the a-dHvA effect was discussed theoretically only in metallic compound LaB_6 by Takayama[37] in detail. In Takayama's study, only the extreme-cross-sectional area of the Fermi surface was treated as a function of deformation by a sound wave. The discerning discussion by Takayama decided the essential term, higher harmonic terms and spin factor are not directly described. It is assumed by calculation that the Zeeman splitting is rather small. For high-field results, we consider response theory reasonable for analyzing experimental results at this stage. Nevertheless, we assume the spin factor to be one significant factor in our analysis.

For useful results using response theory, deformation-potential coupling g_{ij} is proportional to the Grüneisen coefficient:

$$\gamma = \frac{1}{S}\frac{\delta S}{\delta \varepsilon_B} \propto g_{ij},$$

where S, ε, and γ represent the cross-sectional area of the Fermi surface, strain and the Grüneisen coefficient. B shows the applied field. Using deformation coupling g_{ij}, we roughly estimate the Grüneisen coefficient for each Fermi surface independently by response theory. This point is essential in our study.

In GdSb and SmSb, the anomalous field dependence of oscillatory intensity was obtained in the a-dHvA measurement.[9] The intensity of these compounds has some nodes in the C_{11} mode. To explain the anomalous field dependence, a large g factor is evolved. We consider that the enhancement of the g factor is caused by the exchange interaction. To clarify this exchange interaction, it is necessary to measure the g factor directly. For these rare-earth monopnictides, precise measurements of the g factor have not yet been made.

It would be interesting to comment on $Tb_x Y_{1-x} Sb$. In $Tb_x Y_{1-x} Sb$, the CEF energy is adjustable by doping Tb.[38] $Tb_x Y_{1-x} Sb$ is therefore, a suitable substance for the systematic study of the relationship between the CEF and spin splitting of the Fermi surface.[39]

Remaining problems include an inconsistency around the [100] direction in the C_{11} mode. Response theory cannot reproduce the flat region around [100]. We consider that this originates in the assumption of $R_S = 1$. We will report more precisely and this is subject to a future study.

V. SUMMARY

We measured the acoustic dHvA effect in the singlet-ground-state compound TmSb. Observed Fermi surfaces of TmSb are isostructural to the reference compound LaSb. Spin splitting of the α and β surfaces in our acoustic measurement is consistent with previous experiments on oscillatory magnetization. Using the oscillation intensity observed by the C_{11} and C_{44} modes, we obtained angular variation in area coefficients for the α and β surfaces. We analyzed results in terms of the theory of the acoustic dHvA effect, in which deformation, rotation, and multiband terms are considered. The global features of area coefficients are well explained by theory, but fine structures remain to be clarified. A rigorous treatment of the spin factor may be important to the present system. In future research, we plan to study the spin-splitting factor.

[1] See e.g., G. Busch, O. Marincek, A. Menth, and O. Vogt, Phys. Lett. **14**, 262 (1965); S. Forner, B.R. Cooper, and O. Vogt, Phys. Rev. B **6**, 2040 (1972).

[2] J. Rossat-Mignot, P. Burlet, H. Batholin, O. Vogt, and R. Lagnier, J. Phys. C **13**, 6381 (1980).

[3] T. Kasuya, Prog. Theor. Phys. Suppl. **108**, 1 (1992).

[4] F. Hulliger, in *Handbook on the Physics and Chemistry of Rare Earths*, edited by K. A. Gschneider, Jr. and L. Eyring (North-Holland Physics Publishing, Amsterdam, 1979), p. 153.

[5] A. Hasegawa, J. Phys. Soc. Jpn. **54**, 677 (1985).

[6] T. Suzuki, Y. Haga, D.X. Li, T. Matsumura, E. Hotta, A. Uesawa, M. Kohgi, T. Osakabe, S. Takagi, H. Suzuki, T. Kasuya, Y. Chiba, T. Goto, S. Nakamura, R. Settai, S. Sakatsume, A. Ochiai, K. Suzuki, S. Nimori, G. Kido, K. Ohyama, M. Date, Y. Morii, T. Terashima, S. Uji, H. Aoki, T. Naka, T. Matsumoto, Y. Ohara, H. Yoshizawa, Y. Okayama, Y. Okunuki, A. Ichikawa, H. Takahashi, N. Mori, T. Inoue, T. Kuroda, K. Sugiyama, K. Kindo, A. Mitsuda, S. Kimura, S. Takayanagi, N. Wada, A. Oyamada, K. Hayashi, S. Maegawa, T. Goto, Y.S. Kwon, E. Vincent, and P. Bonville, Physica B **206&207**, 771 (1995).

[7] S. Nimori, G. Kido, H. Matsui, T. Goto, D.X. Li, and T. Suzuki, Physica B **201**, 111 (1994).

[8] M. Kataoka and T. Goto, J. Phys. Soc. Jpn. **62**, 4352 (1993).

[9] R. Settai, Ph.D. thesis, Tohoku University, 1990.

[10] R. Settai, T. Goto, S. Sakatsume, Y.S. Kwon, T. Suzuki, Y. Kaneta, and O. Sakai, J. Phys. Soc. Jpn. **63**, 3026 (1994).

[11] T. Goto, H. Matsui, R. Settai, and S. Sakatsume, Physica B **186-188**, 107 (1993).

[12] T. Goto, K. Morita, H. Matsui, S. Nakamura, R. Settai, Y. Haga, T. Suzuki, M. Kataoka, and S. Sakatsume, Physica B **199&200**, 517 (1994).

[13] K. Morita, T. Goto, S. Nakamura, Y. Haga, T. Suzuki, Y. Kaneta, and O. Sakai, Physica B **230-232**, 192 (1997).

[14] T. Goto, K. Morita, S. Nakamura, Y. Nemoto, O. Suzuki, M. Kataoka, and S. Sakatsume, Physica B **219&220**, 86 (1996).

[15] H. Matsui, T. Goto, M. Kataoka, T. Suzuki, H. Harima, S. Kunii, R. Takayama, and O. Sakai, J. Phys. Soc. Jpn. **64**, 3315 (1995).

[16] G. Busch, A. Menth, O. Vogt, and F. Hulliger, Phys. Lett. **19**, 622 (1966).

[17] O. Vogt and B.R. Cooper, J. Appl. Phys. **39**, 1202 (1968).

[18] B.R. Cooper and O. Vogt, Phys. Rev. **1**, 1211 (1970).

[19] S. Nimori, G. Kido, D.X. Li, Y. Haga, and T. Suzuki, J. Magn. Magn. Mater. **140-144**, 1167 (1995).

[20] D.X. Li, Y. Haga, H. Shida, T. Suzuki, A. Kido, S. Nimori, and G. Kido, Physica B **199&200**, 609 (1994).

[21] D.X. Li, Y. Haga, H. Shida, T. Suzuki, Y.S. Kwon, S. Nimori, and G. Kido, J. Magn. Magn. Mater. **140-144**, 1165 (1995).

[22] G. Kido, S. Nimori, and Y. Nakagawa, Sci. Rep. Res. Inst. Tohoku Univ. A **38**, 338 (1993).

[23] S. Nimori, A. Kido, G. Kido, Y. Nakagawa, Y. Haga, and T. Suzuki, Physica B **186-188**, 173 (1993).

[24] A. Kido, S. Nimori, G. Kido, Y. Nakagawa, Y. Haga, and T. Suzuki, Physica B **186-188**, 185 (1993).

[25] M.E. Mullen, B. Lüthi, P.S. Wang, E. Bucher, L.D. Longinotti, J. Maita, and H.R. Ott, Phys. Rev. B **10**, 186 (1974).

[26] R.J. Birgeneau, E. Bucher, L. Passell, and K.C. Tuberfield, Phys. Rev. B **4**, 718 (1971).

[27] R.J. Birgeneau, in *Magnetism and Magnetic Materials—1972*, edited by C. D Graham, Jr. and J. J. Rhyne, AIP Conf. Proc. No. 10 (AIP, New York, 1973), p. 1664.2.

[28] D.B. McWhan, C. Vettier, R. Youngblood, and G. Shirane, Phys. Rev. B **20**, 4612 (1979).

[29] K.C. Tuberfield, L. Passell, R.J. Birgeneau, and E. Bucher, J. Appl. Phys. **42**, 1746 (1971).

[30] K. Sugawara, C.Y. Huang, and B.R. Cooper, Phys. Rev. B **11**, 4455 (1975).

[31] S. Nimori, G. Kido, D.X. Li, and T. Suzuki, Physica B **211**, 148 (1995).

[32] T. Goto, T. Suzuki, A. Tamaki, Y. Ohe, S. Nakamura, and T. Fujimura, Bull. Res. Inst. Sci. Meas. **35**, 46 (1989) (in Japanese).

[33] T. Goto, A. Sawada, and S. Sakatsume, Jpn. J. Appl. Phys., Part 1 **8**, 157 (1993).

[34] S. Sakatsume, H. Matsui, R. Settai, S. Nakamura, Y. Ohtani, S. Kasahara, and T. Goto, Physica B **186-188**, 165 (1993).

[35] R. Settai, M. Chida, S. Yanagida, and T. Goto, Jpn. J. Appl. Phys., Part 1 **31**, 3736 (1992).

[36] R. Settai, T. Goto, S. Sakatsume, Y.S. Kwon, T. Suzuki, and T. Kasuya, Physica B **186-188**, 176 (1993).

[37] R. Takayama, Ph.D. thesis, Tohoku University, 1980.

[38] B.R. Cooper and O. Vogt, Phys. Rev. B **1**, 1218 (1970).

[39] T. Sakon, Y. Nakanishi, M. Ozawa, H. Nojiri, T. Suzuki, and M. Motokawa, J. Magn. Magn. Mater. **177−181**, 355 (1998).